JOURNAL OF PROPULSION AND POWER
Vol. 19, No. 5, September–October 2003

# Premixed Flame Kinematics in a Longitudinal Acoustic Field

Doh-Hyoung Lee* and Tim C. Lieuwen†
*Georgia Institute of Technology Atlanta, Georgia 30332-0150*

**The occurrence of self-excited, combustion-driven oscillations poses significant problems in premixed combustors. The interactions between flames and longitudinal acoustic oscillations play a key role in many of these instabilities. Prior analytical investigations of these interactions have shown that the dominant parameter controlling the response of the flame area fluctuations to acoustic velocity perturbations is a Strouhal number based on flame length and axial flow velocity. These analyses assumed that the acoustic disturbances remain one dimensional, even in the near field of the flame. Basic acoustic considerations and analyses show, however, that the acoustic velocity field exhibits two-dimensional features near the flame front (Lee, D. H., and Lieuwen, T., "Acoustic Nearfield Characteristics of a Conical, Premixed Flame," *Journal of the Acoustical Society of America*, Vol. 113, No. 1, 2003). This paper investigates how the multidimensionality of the acoustic field affects the flame's response to velocity perturbations. The transfer function relating flame area fluctuations to acoustic velocity perturbations is calculated numerically and compared with analytical, one-dimensional results. In addition to the Strouhal number, these more general results depend upon the temperature ratio across the flame, the diameter ratio of the rapid expansion, and the ratio of flame length to duct diameter. It is shown that the flame transfer function is qualitatively similar in many cases, however, and that the Strouhal number remains the dominant parameter affecting the calculated transfer function. Analysis reveals that the differences between the two calculations arise from gas compressibility in the flame region and spatial nonuniformity (not two-dimensionality) in the acoustic velocity along the flame front. These results clarify the reasons behind the rather unexpected agreement between the simplified one-dimensional theory and the measurements of Ducruix et al. (Ducruix, S., Durox, D., and Candel, S., "Theoretical and Experimental Determinations of the Transfer Function of a Laminar Premixed Flame," *Proceedings of the Combustion Institute*, Vol. 28, 2000).**

## Nomenclature

$A_f$ = flame area
$C$ = defined in Eq. (8)
$c$ = speed of sound
$G$ = Green's function
$k$ = wave number
$L$ = flame length (see Fig. 1)
$M$ = Mach number
$n$ = unit outward normal
$p'$ = acoustic pressure
$Q$ = heat-release or volume flow rate
$R$ = radius of combustor
$\mathcal{R}$ = reflection coefficient
$r$ = radial coordinate
$S$ = boundary surface
$Sr$ = Strouhal number, $(\omega L/\bar{U})[1 + (R/L)^2]$
$S_u$ = laminar flame speed
$T$ = temperature
$\bar{U}$ = axial mean-flow velocity
$u'$ = axial acoustic velocity
$\bar{V}$ = radial mean-flow velocity
$v'$ = transverse acoustic velocity
$\boldsymbol{x}$ = position vector
$\gamma$ = specific heats ratio
$\Delta$ = boundary element width
$\lambda$ = wavelength
$\rho$ = density
$\Phi$ = flame transfer function
$\omega$ = angular frequency

*Subscripts and Superscripts*

$b$ = moving flame base contribution in flame transfer function
$n$ = normal to flame
$s$ = boundary surface-radial coordinate
$w$ = flame wrinkling contribution to flame transfer function
1 = unburned region
2 = burned region
$\hat{}$ = nondimensional variable
$'$ = temporal fluctuating value of variable
$\bar{}$ = temporal mean value of variable

Received 21 May 2002; revision received 20 January 2003; accepted for publication 5 May 2003. 

*Graduate Research Assistant, School of Aerospace Engineering.
†Assistant Professor, School of Aerospace Engineering. Member AIAA.

## Introduction

COMBUSTION instabilities often pose significant problems in the development and operation of combustion systems for propulsion or power generation.[1] The interactions between flames and longitudinal acoustic oscillations play a key role in many of these instabilities. In these systems acoustic oscillations with frequencies closely related to natural acoustic modes of the chamber impinge upon the flame, whereupon they are partially reflected and transmitted by the sudden change in gas properties at the flame front. The flow and pressure oscillations accompanying these acoustic waves disturb the flame's position and local reaction rate and often cause additional heat-release oscillations. These heat-release oscillations can add or remove energy from the local acoustic field, depending upon their relative phasing.

Crucial to modeling these oscillations is an adequate description of the interactions between the incident acoustic waves and the flame front. Noting the disparity between the length scales of typical flame thicknesses and acoustic waves, a number of studies have modeled these interactions by treating the flame as a surface of discontinuity separating cold reactants and hot products. Following Markstein,[2] one can then derive kinematical relations for the flame-front position, as well as mass, momentum, and energy conservation conditions that couple the up and downstream flowfields. Such flame kinematics models have been pursued by Marble and Candel,[3] Yang and Culick,[4] Dowling,[5] and Fleifil et al.[6]

To calculate the flame's response to the acoustic disturbances, such models require the characteristics of the acoustic field at all points along the flame surface. The preceding studies have specified the local acoustic field by assuming that the disturbances remain axially uniform and/or one-dimensional, even in the near field of the flame. Although the assumption of a planar acoustic field is reasonable at a sufficient distance from the flame, it does not accurately account for the multidimensional characteristics of the acoustic field near the flame itself.

To illustrate, consider a flame in a two-dimensional duct with rigid walls that is excited by a plane, harmonically oscillating wave. Assume that the wavelength of the disturbance $\lambda$ is large enough so that no propagating transverse duct modes of the combustor are excited. After impinging upon the flame, this wave is scattered, and longitudinal waves are reflected and transmitted up and downstream, respectively. In addition to these planar waves, multidimensional oscillations composed of "evanescent," nonpropagating waves are also excited.[7] Consequently, the acoustic near field of the flame is composed of a complex superposition of the three propagating waves and the evanescent waves. However, these evanescent waves only have a local effect on the acoustic fields because they decay exponentially with distance from the flame. Thus, the acoustic field is one dimensional at sufficiently large distances away from the flame, being composed of the incident, reflected, and transmitted propagating plane waves.

Quantitative calculations have confirmed this qualitative picture of the flame's acoustic near field.[8] For example, recent numerical analyses of the authors[1] have shown that the acoustic velocity field exhibits significant two-dimensional features at the flame front (results also presented later). This two dimensionality arises from geometric effects and the large temperature jump across the flame surface that is oriented obliquely to the incident planar waves. Because the flame is being forced by these local, two-dimensional velocity oscillations, it is not clear that one-dimensional analyses contain reasonable fidelity to describe the studied interactions adequately.

Recently, however, Ducruix et al.[9] have compared the predictions of a similar one-dimensional acoustic model with experiments. In these experiments a premixed Bunsen flame was excited by upstream acoustic disturbances. The resultant heat-release fluctuations were characterized using measurements of global CH* emissions. They computed a transfer function between these chemiluminescence oscillations and the measured velocity at the base of the flame and found good agreement between the data and one-dimensional theory for low flame Strouhal numbers.

This good agreement suggests that a laminar flame's response to acoustic disturbances can be reasonably captured by a rather simple model and, furthermore, that multidimensional acoustic effects upon overall heat release might not be significant. It is this latter point that is the subject of this paper. Specifically, this paper compares the flame area-acoustic velocity transfer function predictions of one-dimensional approaches with those computed by a two-dimensional solver and determines the regimes under which they do and do not give similar results. The following Acoustic Field Analysis section briefly describes this numerical approach and its principal assumptions. Then, the Flame Response Analysis section uses computed results of the acoustic velocity at the flame front as inputs to the flame-dynamics models developed in Refs. 6 and 9 but retains the neglected multidimensional effects. It is shown that the two calculations are in agreement over a significant parameter space. The paper concludes with an analysis of the flame-dynamics equations to develop a better understanding of this (unexpected) agreement.

## Acoustic Field Analysis

### Geometry

The investigated geometry is shown in Fig. 1. It consists of an axisymmetric domain, where a premixed flame of length $L$ is located at the rapid expansion plane between two ducts of diameters $D_1$ and $D_2$. This geometry closely resembles that found in a range of laboratory and industrial hardware, such as Bunsen burners, ramjets, and some furnace designs. In addition, it contains many of the dominant features of more complex hardware. For example, modern low-emissions gas turbine combustors generally consist of several small premixers transitioning into a much larger can or annular combustor.[10]

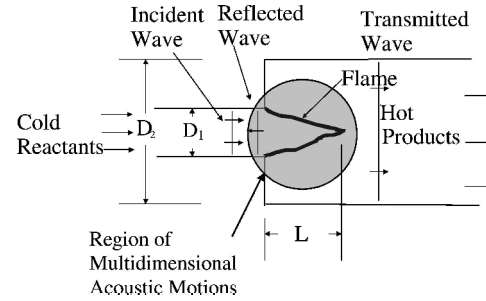


**Fig. 1 Schematic of investigated configuration for case where disturbance originates from upstream.**

The flame's mean position is assumed to be conical. This shape closely resembles that typically observed in this geometry in flows with low to moderate amounts of swirl in the mean flow.[11] In reality, nonuniformities in mean-flow profile and flame propagation speed cause deviations in the flame from a conical shape. However, the differences in acoustic field structure are small, as long as these deviations in shape are small relative to the other characteristic lengths in the problem: the duct diameters, flame length, and acoustic wavelength.

### Jump Conditions

Given the disparity in length scales between flame thickness and acoustic wavelength, we treat the flame front as a surface of temperature discontinuity, and no additional entropy production occurs outside of it. Such an approximation is routinely used in the combustion literature[12] and is satisfied to a high degree of accuracy for the frequencies of interest here [e.g., the thickness of a stoichiometric methane—air flame is about 1 mm; acoustic wavelengths for frequencies of interest are typically on the order of 1 m (Ref. 11)].

The linearized jump conditions across the flame front can be derived using the mass, momentum, and energy conservation equations. The following expressions are derived in Lieuwen,[13] where terms of the order of the mean-flow Mach number squared and the ratio of the flame thickness to acoustic wavelength are neglected:

Normal momentum:

$$p_1'/\bar{p} = p_2'/\bar{p} \tag{1}$$

Energy:

$$u_{n,2}'/\overline{c_1} - u_{n,1}'/\overline{c_1} = M_s(T_2/T_1 - 1)\{-[(\gamma - 1)/\gamma](p_1'/\bar{p}) + S_1'/\overline{S_1}\} \tag{2}$$

The variables $u_n$, $p$, $M_s$, $c$, $\gamma$, $T_2/T_1$, and $S$ denote the normal velocity, pressure, mean flame speed Mach number relative to the unburned gas, sound speed, specific heats ratio, temperature ratio across the flame, and flame speed, respectively. Note that the fluctuating flame speed is, in general, a function of the fluctuating pressure, temperature, and flow strain rate. The unsteady terms not only consist of acoustic fluctuations, but the superposition of the acoustic, entropy, and vorticity modes. The mass and tangential momentum conditions are also derived in Ref. 13 but are not considered here because within the approximations of this analysis they are only needed to solve for the characteristics of the entropy and vorticity modes (see Refs. 2 and 13 for further discussion).

Consider the magnitudes of the terms on the right side of Eq. (2), which quantify the jump in normal velocity across the flame. The first term is $\mathcal{O}(M_s)$ relative to those on the left, assuming that $p' \sim \bar{\rho}\bar{c}u'$. Assuming that the normalized flame speed and pressure perturbations are also of similar magnitude as McIntosh's analysis suggests,[14] that is, $S_1'/\overline{S_1} \sim \mathcal{O}(p_1'/\bar{p})$, then the second term on the

right is also of $\mathcal{O}(M_s)$. Typical values of $M_s$ are very low, for example, the flame speed of a stoichiometric methane-air mixture is about 40 cm/s (Ref. 11). Using an upstream temperature of 300 K, this corresponds to an $M_s$ value of 0.001. As such, we neglect these terms in this analysis so that the jump conditions across the flame are

$$p'_1 = p'_2 \tag{3}$$

$$u'_{n,2} = u'_{n,1} \tag{4}$$

This assumption requires careful consideration because the neglected terms are responsible for unsteady heat addition and, thus, amplification or damping of the acoustic field by the acoustic-flame interaction. Thus, it might appear that their neglect completely removes the interesting physics from the problem. However, these unsteady heat-release terms can be calculated to good accuracy using these solutions and standard perturbation procedures. To illustrate, denote the terms on the right side of Eq. (2) as $M_s\psi(p', u', \ldots)$ and expand the unsteady fields about their value in the limit of vanishing right-hand side of Eq. (2), for example, $u' = u'_0 + M_s u'_1 + \ldots$. The leading-order heat-release perturbation $\psi(p'_0, u'_0, \ldots)$ can then be determined from the expansion $M_s\psi(p', u', \ldots) = M_s\psi(p'_0, u'_0, \ldots) + M_s^2[p'_1(\partial\psi/\partial p')|_{p'_0} + u'_1(\partial\psi/\partial u')|_{u'_0}] + \ldots$. Invoking Eq. (4) is useful because it allows for generation of general results that are independent of the details of the heat-release model that is used.

This approximation is well supported by experiments. Data presented by Lieuwen[15] and Poinsot et al.[16] show that the pressure amplitude growth rates during an instability are on the order of 1%, implying that the real part of the right side of Eq. (2) is small. In addition, measurements reported by Lovett and Uznanski[17] show that the frequency shift induced by the unsteady heat release is less than 10%, indicating that the imaginary part of the right side of Eq. (2) is also small.

Several other points should be noted. First, although the flame front is moving as a result of the acoustic perturbations, for this linear analysis the matching conditions given by Eqs. (3) and (4) are applied at the mean flame location. As such, the analysis is only valid when the flame deviation about its mean shape is small. This can be anticipated to pose some difficulties for comparison of the acoustic field calculations with experiments because the flame front exhibits substantial oscillations, even for relatively low values of acoustic velocity (e.g., see the images in Ref. 9). This is because the relative flame displacement about its mean value is related to the ratio $u'_n/\bar{u}_n$. The $u'_n/\bar{u}_n$ ratio appears to have been appreciable in prior experimental studies, apparently because of the need for large enough acoustic amplitudes to obtain sufficient signal levels.[9,18]

Second, the velocity in Eqs. (2) and (4) refers, in general, to the sum of the acoustic and vortical components, that is, these disturbance modes are coupled at the flame front where they have similar magnitudes. It is assumed here that the normal vortical velocity component is small relative to that of the acoustic component and, thus, is neglected. Because of the substantially shorter wavelength of the vortical component and its solenoidal character, its normal component is of the order of the flame speed Mach number relative to that of the normal acoustic velocity.[13] The tangential components of the vortical and acoustic perturbations are of similar magnitude, however. Analysis that fully includes this vortical-acoustic coupling shows that it results in an acoustic damping term that is $\mathcal{O}(M_s)$ (Ref. 13).

**Acoustic Field**

As just noted, we assume that the acoustic field is divided into two isentropic regions (of differing mean properties) up and downstream of the flame, which are coupled across the flame front. As such, these wave motions are described by the classical, isentropic wave equation. We assume that the mean-flow Mach number of the burned and unburned gases is low and, thus, neglect convection effects on these wave motions. As such, the following Helmholtz equations describe the harmonic wave motions in the regions up and downstream of the flame[7] at an angular frequency $\omega$:

Upstream of flame:

$$\nabla^2 p' + k_1^2 p' = 0 \tag{5}$$

Downstream of flame:

$$\nabla^2 p' + k_2^2 p' = 0 \tag{6}$$

where $k = \omega/c$ is the wave number. The equivalent integral form of Eqs. (5) or (6), the Helmholtz integral equation, is given by[7]

Upstream of flame

$$p'(\boldsymbol{x})C(\boldsymbol{x}) = -\iint_S [i\omega\overline{\rho_1}\boldsymbol{u}'(\boldsymbol{x}_s)G(\boldsymbol{x}_s, \boldsymbol{x}) - p'(\boldsymbol{x}_s)\nabla G(\boldsymbol{x}_s, \boldsymbol{x})]\cdot\boldsymbol{n}_1\,\mathrm{d}S \tag{7}$$

Downstream of flame

$$p'(\boldsymbol{x})C(\boldsymbol{x}) = -\iint_S [i\omega\overline{\rho_2}\boldsymbol{u}'(\boldsymbol{x}_s)G(\boldsymbol{x}_s, \boldsymbol{x}) - p'(\boldsymbol{x}_s)\nabla G(\boldsymbol{x}_s, \boldsymbol{x})]\cdot\boldsymbol{n}_2\,\mathrm{d}S \tag{8}$$

where $\boldsymbol{x}$, $\boldsymbol{x}_s$, $\boldsymbol{u}'$, and $\boldsymbol{n}$ denote the measurement point, boundary surface point (consisting of the closed region demarcated by the flame front, combustor wall, and up or downstream boundary), acoustic velocity vector, and unit normal vector pointing out of the respective domain. Also, $G$ is the free-space Green's function $G = e^{-ik|\boldsymbol{x}-\boldsymbol{x}_s|}/(4\pi|\boldsymbol{x}-\boldsymbol{x}_s|)$. It can be shown that $C(x) = \frac{1}{2}$, 1, and 0 for smooth boundary points, interior domain, and exterior domain points, respectively. (The interior domain is defined as the region inside of the ducts.) The time dependence of the harmonic oscillations is given by $e^{i\omega t}$.

Similar to the acoustic-vortical coupling at the flame, the velocity disturbance modes are coupled at the rapid expansion point where their magnitudes are similar. This coupling can be handled analytically by imposing a Kutta condition at the rapid expansion, for example, see Crighton[19] or Howe.[20] This vorticity generation results in an $\mathcal{O}(M)$ modification to the acoustic field structure in the vicinity of this point and acoustic damping.[21] This effect is neglected in this analysis, consistent with our prior neglect of $\mathcal{O}(M)$ terms. If the position of the flame attachment point does not move in response to oscillations, then even if this effect were retained it would not exert much impact on the dynamics of the flame because it confined to the vicinity of the rapid expansion point. This flame base condition is likely satisfied in well-stabilized flames, but not in flames near the point of blowout, and has been used in several prior studies.[6,9]

The solution of Eqs. (7) and (8) requires specifying the value of the pressure or normal velocity over the surface of integration, that is, $p'(\boldsymbol{x}_s)$ or $\boldsymbol{u}'(\boldsymbol{x}_s)\cdot\boldsymbol{n}$. The jump conditions derived in the prior section are used to couple the acoustic field across the flame, while the normal velocity at the combustor side walls was set to zero. Thus, this problem reduces to that of solving two coupled integral equations for the pressure. The velocity is then determined from the calculated pressure using the linearized Euler equation.

The boundary-element method (BEM) was used to numerically solve the coupled integral equations. Except for points where $|\boldsymbol{x}-\boldsymbol{x}_s| \sim 0$, integrals were evaluated using a four-point Gaussian quadrature scheme. Integration in the vicinity of the singular point $|\boldsymbol{x}-\boldsymbol{x}_s| \sim 0$ was performed analytically using a Taylor-series expansion of the Green's function. Details of implementation of the BEM are described in Refs. 22 and 23. Comparison of the numerical solutions with exact and approximate analytical solutions showed that errors in pressure magnitude were less than 1% when $k_1\Delta < 0.15$.

Results were obtained for two cases, where the incident wave orginates from up or downstream of the flame. To focus on the acoustic field induced by this wave, nonreflecting boundary conditions were imposed on the opposite boundary. These boundary conditions ensured that the reflected and transmitted waves propagate out of the solution domain without additional reflections. Note that calculations of the flame response in a more general longitudinal acoustic field can be constructed from an appropriate combination of these two considered canonical cases. Calculations were performed

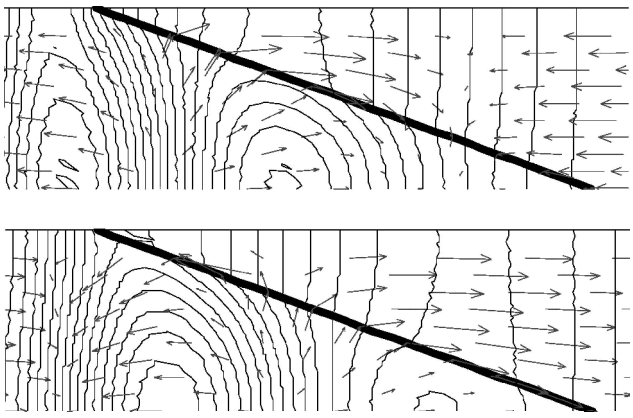

**Fig. 2 Instantaneous pressure isobars and velocity vectors for parameter values $L/\lambda_1 = 1.59$, $L/D_1 = 1.59$, $D_2/D_1 = 1$, and $T_2/T_1 = 6.67$. Incident wave originates from upstream.**

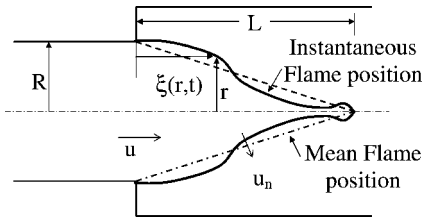


**Fig. 3 Schematic illustrating variables used to characterize flame region.**

only for frequencies below the duct cutoff frequencies, that is, below the frequency of the first radial mode. (Because the domain is axisymmetric, the lowest order transverse mode, an azimuthal one, is not excited).

Figure 2 illustrates a typical result and plots the instantaneous acoustic velocity vectors and pressure isobars through four phases of a cycle. This figure plots the top half of the computed domain, where the top line is the combustor wall, the bottom line is the axis of symmetry, and the slanted line denotes the mean flame-front location. The figure demonstrates the multidimensional nature of the acoustic velocity at the flame front. For instance, the unsteady flow is bent in the normal direction of the flame front on its upstream side by the sudden temperature jump. These two-dimensional features are more pronounced on the upstream side of the flame because of the significantly lower temperature and, hence, shorter wavelength than downstream.

Other calculations not shown here demonstrate that these two-dimensional features are also enhanced for shorter wavelengths relative to the flame length (i.e., larger $L/\lambda_1$) or longer flames relative to the duct radius (i.e., smaller $L/D_1$)[1] (see Ref. 8).

## Flame-Response Calculations

This section describes an analysis of the flame response to the flow oscillations using the BEM calculations just described. The approach and assumptions used here are similar to those of prior analyses[6,9] (with the exception of retaining two-dimensional effects) in order to facilitate comparison. The starting point is the following kinematic relation describing the flame position (assumed to be a single valued function of the radial coordinate) as a function of the flow velocity and flame speed[2]:

$$\frac{\partial \xi}{\partial t} = u - v\frac{\partial \xi}{\partial r} - S_u\sqrt{\left(\frac{\partial \xi}{\partial r}\right)^2 + 1} \tag{9}$$

where $\xi(r, t)$, $u$, $v$, and $S_u$ are axial flame displacement (see Fig. 3), axial velocity, radial velocity and flame speed relative to the unburned gases, respectively. We next decompose the variables into their mean and fluctuating parts and retain only linear terms in perturbations. As in Refs. 6 and 9, it is assumed that the flame speed is constant.

$$0 = \bar{U} - \bar{V}\frac{\mathrm{d}\bar{\xi}}{\mathrm{d}r} - S_u\sqrt{1 + \left(\frac{\mathrm{d}\bar{\xi}}{\mathrm{d}r}\right)^2} \tag{10}$$

$$\frac{\partial \xi'}{\partial t} = u' - v'\frac{\mathrm{d}\bar{\xi}}{\mathrm{d}r} - \bar{V}\frac{\partial \xi'}{\partial r} - S_u\left[\frac{\mathrm{d}\bar{\xi}}{\mathrm{d}r}\frac{\partial \xi'}{\partial r}\Big/\sqrt{1 + \left(\frac{\mathrm{d}\bar{\xi}}{\mathrm{d}r}\right)^2}\right] \tag{11}$$

All variables are nondimensionalized using the relations $\hat{\xi}'(\hat{r}) = \xi'/L$, $\hat{r} = r/R$, $\hat{u}' = u'/U$, $\hat{v}' = v'/U$, $G_\omega = \omega R/S_u$, and

$$f(\hat{r}) = \frac{\bar{V}}{S_u} + \frac{\mathrm{d}\bar{\xi}}{\mathrm{d}r}\Big/\sqrt{1 + \left(\frac{\mathrm{d}\bar{\xi}}{\mathrm{d}r}\right)^2}$$

Assuming harmonic oscillations at an angular frequency $\omega$, Eq. (11) becomes an ordinary differential equation that can be solved for the flame position. The solution takes the following form:

$$\hat{\xi}' = \hat{\xi}'(1)\exp\left[iG_\omega\int_{\hat{r}}^{1} 1/f(\eta)\,\mathrm{d}\eta\right] + \exp\left[-iG_\omega\int_0^{\hat{r}} 1/f(\eta)\mathrm{d}\eta\right]$$
$$\times\int_1^{\hat{r}}\left\{\left(\hat{u}' - \hat{v}'\frac{\mathrm{d}\bar{\xi}}{\mathrm{d}r}\right)\frac{\bar{U}}{S_u}\frac{R}{L}\Big/f(\eta)\cdot\exp\left[iG_\omega\int_0^{\eta} 1/f(\rho)\,\mathrm{d}\rho\right]\right\}\mathrm{d}\eta \tag{12}$$

Further progress in analyzing this equation requires specification of the mean flame-front position $\bar{\xi}$. As just noted, we assume a conical flame position:

$$\frac{\mathrm{d}\bar{\xi}}{\mathrm{d}r} = -\frac{L}{R}, \qquad \frac{\bar{U}}{S_u} = \sqrt{1 + \left(\frac{L}{R}\right)^2} \tag{13}$$

Inserting these relations into Eq. (12), we obtain

$$\hat{\xi}' = \hat{\xi}'(1)\exp[iSr(\hat{r} - 1)]$$
$$+ \frac{R^2 + L^2}{L^2}\exp(iSr\hat{r})\int_{\hat{r}}^{1}\hat{u}_n'\frac{\bar{U}}{S_u}\cdot\exp(-iSr\rho)\,\mathrm{d}\rho \tag{14}$$

where $\hat{u}_n'(\equiv u_n'/\bar{U})$ is the nondimensionalized fluctuating velocity normal to the mean flame-front position (as opposed to its instantaneous position) and $Sr$ is the Strouhal number, defined as $Sr = (\omega L/\bar{U})[1 + (R/L)^2]$. This Strouhal number $Sr$ was referred to as the reduced frequency $\omega^*$ by Ducruix et al.[9] If the acoustic velocity is assumed to only have an axial component that does not vary spatially, Eq. (14) is identical to that obtained by Ducruix et al.[9]

Following Fleifil et al.[6] and Ducruix et al.,[9] the global heat-release rate of the flame is written as

$$Q(t) = \rho S_u A_f \Delta q_r \tag{15}$$

where $\Delta q_r$ is the heat of reaction. In general, fluctuations in each of these quantities can contribute to heat-release oscillations, that is,

$$Q'/\bar{Q} = \rho'/\bar{\rho} + S_u'/\overline{S_u} + A_f'/\overline{A_f} + \Delta q_r'/\overline{\Delta q_r} \tag{16}$$

As in Refs. 6 and 9, we focus on the effects of flame area fluctuations, that is, on the characteristics of the $A_f'/\overline{A_f}$ term. The instantaneous flame area is

$$A_f = \int_0^R 2\pi r\sqrt{1 + \left(\frac{\partial \xi}{\partial r}\right)^2}\,\mathrm{d}r \tag{17}$$

The instantaneous flame area is decomposed into mean and fluctuating parts. Substituting Eq. (14) into the linearized area fluctuation term from Eq. (17) yields

$$\frac{A'_f}{\overline{A_f}} = \frac{2L^2}{R^2+L^2}\left[\int_0^1 \hat{\xi}'\,\mathrm{d}\hat{r} - \hat{\xi}'(1)\right]$$

$$= 2\int_0^1 \exp(iSr\hat{r})\left[\int_{\hat{r}}^1 \hat{u}'_n \frac{\bar{U}}{S_u}\exp(-iSr\eta)\,\mathrm{d}\eta\right]\mathrm{d}\hat{r}$$

$$+ \frac{2L^2}{R^2+L^2}\hat{\xi}'(1)\left[\frac{1-\exp(-iSr)}{iSr} - 1\right] \tag{18}$$

Note the two contributions to the flame area fluctuation: flame wrinkling and movement of the flame anchoring point.

$$\frac{A'_f}{\overline{A_f}} = \left.\frac{A'_f}{\overline{A_f}}\right|_w + \left.\frac{A'_f}{\overline{A_f}}\right|_b \tag{19}$$

The displacement of the flame base can be related to its velocity by

$$\hat{\xi}'(1) = u'_{\mathrm{base}}/i\omega L \tag{20}$$

where $u'_{\mathrm{base}}$ denotes the axial velocity of the flame base (not the flow velocity).

Substituting Eq. (20) into Eq. (18), the normalized flame transfer function caused by the flame base movement $\Phi_b$ can be expressed as a function of the Strouhal number.

$$\Phi_b = \frac{A'_f/A_f|_b}{u'_{\mathrm{base}}/\bar{U}} = \frac{2}{Sr^2}[\exp(-iSr) - 1 + iSr] \tag{21}$$

Consider now the contribution from flame wrinkling $A'_f/\overline{A_f}|_w$.

$$\left.\frac{A'_f}{\overline{A_f}}\right|_w = \frac{2i}{Sr}\frac{\bar{U}}{S_u}\left[\int_0^1 \hat{u}'_n(\hat{r})\exp(-iSr\hat{r})\,\mathrm{d}\hat{r} - \int_0^1 \hat{u}'_n(\hat{r})\,\mathrm{d}\hat{r}\right] \tag{22}$$

The first term in Eq. (22) is related to the correlation between the unsteady normal acoustic velocity and the harmonic term, $\exp(-iSr\hat{r})$, whose spatial variation occurs over a convective wavelength. The second term is simply an integral of the unsteady velocity over the flame front.

Ducruix et al.'s[9] result can be recovered when $\hat{u}'_n$ only has a contribution from a constant axial velocity $\hat{u}'$ (i.e., $\hat{u}'_r = 0$):

$$\Phi_{w,1-D} = \frac{A'_f/\overline{A_f}|_{w,1-D}}{u'_x/\bar{U}} = \frac{2}{Sr^2}[1 - iSr - \exp(-iSr)] \tag{23}$$

Note that, with the exception of a sign difference, Eqs. (21) and (23) are identical. Thus, the total flame area fluctuation term is zero if the axial acoustic velocity $u'$ and flame-base velocities $u'_{\mathrm{base}}$, are equal. In this case the flame simply moves back and forth in a bulk motion with a constant surface area.

We next compare our computed results of the transfer function between flame area and acoustic velocity oscillations to the one-dimensional result, Eq. (24). Because the acoustic velocities in our calculations vary spatially, such a comparison requires specifying a reference velocity (e.g., the velocity at a particular point) to use in determining this transfer function. We used the following method for determining this reference velocity: Because the computed acoustic pressure and velocity are one dimensional far upstream or downstream of the flame for the frequencies considered here (i.e., below the duct cutoff frequency), the amplitude of the reflected plane wave can be determined through the plane-wave relations:

If wave is incident from upstream:

$$p'(x,t) = \bar{\rho}_1\bar{c}_1 u'_i\left\{e^{i(\omega t - ikx)} + \Re e^{i(\omega t + kx)}\right\}$$

$$u'(x,t) = u'_i\left\{e^{i(\omega t - kx)} - \Re e^{i(\omega t + kx)}\right\} \tag{24}$$

If wave is incident from downstream:

$$p'(x,t) = -\bar{\rho}_2\bar{c}_2 u'_i\left\{e^{i(\omega t + kx)} + \Re e^{(i\omega t - ikx)}\right\}$$

$$u'(x,t) = u'_i\left\{e^{i(\omega t + kx)} - \Re e^{i(\omega t - kx)}\right\} \tag{25}$$

where $\Re$ and $u'_i$ are the plane-wave reflection coefficient and velocity amplitude of the incident plane wave, respectively. The reference velocity was calculated from Eq. (24) or Eq. (25) at the flame base, $x = 0$, that is,

$$u'_{\mathrm{ref}} = u'_i(1 - \Re) \tag{26}$$

Thus, the computed transfer function $\Phi_w$ is given by

$$\Phi_w = \frac{A'_f/\overline{A_f}|_w}{u'_{\mathrm{ref}}/\bar{U}} \tag{27}$$

Selecting the reference reflection position necessarily introduces an additional, somewhat artificial, dependence of the flame transfer function upon wavelength of the incident wave. For example, in a straight geometry a more suitable location for the "origin" of the reflected plane wave is at the location $x_{\mathrm{ref}} = L/3$. Because we use a different origin, the phase of the reflection coefficient is modified by the factor $\exp(2ikx_{\mathrm{ref}})$, which exhibits a linear phase dependence upon $x_{\mathrm{ref}}/\lambda$. The amplitude of the reflection coefficient is independent of this choice of origin of the reflected wave.

To facilitate comparison of transfer function results for cases where the incident wave comes from up or downstream of the flame, it is useful to define the modified transfer function $\Phi_{w2}$:

If wave is incident from upstream:

$$\Phi_{w2} = \Phi_w \tag{28}$$

If wave is incident from downstream:

$$\Phi_{w2} = \Phi_w(D_2/D_1)^2 \tag{29}$$

This transformation is useful in cases where the incident wave originates from downstream because the acoustic velocity is amplified by the area contraction, whereas the reference velocity is still calculated from the reflection coefficient.

If the acoustic field is uniform and one dimensional, Eq. (23) shows that the transfer function between the non dimensional flame area and velocity fluctuations is only a function of the Strouhal number. In general, this transfer function is controlled by several additional parameters that affect the characteristics of the acoustic field. Although alternative groupings are possible, we express our results in terms of the Strouhal number and the four parameters: $T_2/T_1$, $L/\lambda_1$, $L/D_1$, and $D_2/D_1$. If there is no expansion, that is, $D_2/D_1 = 1$, the one-dimensional results are exact if $T_2/T_1 = 1$ or if $L/D_1 = 0$. For reference, using a frequency, flame length, mean-flow velocity, and sound speed of 100 Hz, 10 cm, 30 m/s, and 330 m/s, respectively, the parameters $L/\lambda_1$ and $\omega L/U$ equal 0.03 and 2.1, respectively. We next present results illustrating the dependence of $\Phi_{w2}$ upon these parameters.

Figure 4 plots the predicted dependence of $\Phi_{w2}$ upon Strouhal number for a straight geometry at several $L/\lambda_1$ and $L/D_1$ values. Also shown on the figure are the one-dimensional acoustic predictions, taken from Eq. (23). Comparisons of the one- and two-dimensional calculations show quantitative, but not qualitative, differences in the amplitude of the transfer function for $Sr < 10$. For larger Strouhal numbers these two results differ from each other by a nearly constant factor. Note that the phase transfer function in the $L/\lambda_1 = 0.1$ and 0.5 cases look similar except for a constant phase offset. This phase offset is caused by the choice-of-reference reflection position, discussed earlier (in this case it would be nearly removed if $x_{\mathrm{ref}} = L/3$ were used). The lower frequency case ($L/\lambda_1 = 0.1$) shows some differences at low Strouhal number, but increasing agreement at higher Strouhal number. The primary difference between the two calculations lies in the enhanced oscillatory nature

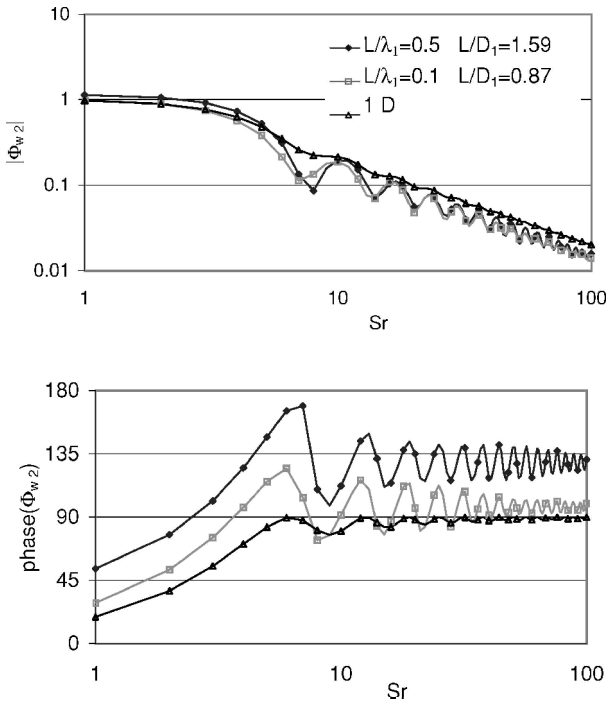


**Fig. 4 Dependence of magnitude and phase of flame transfer function upon Strouhal number ($T_2/T_1$ = 6.67 and $D_2/D_1$ = 1). Incident wave originates from upstream.**

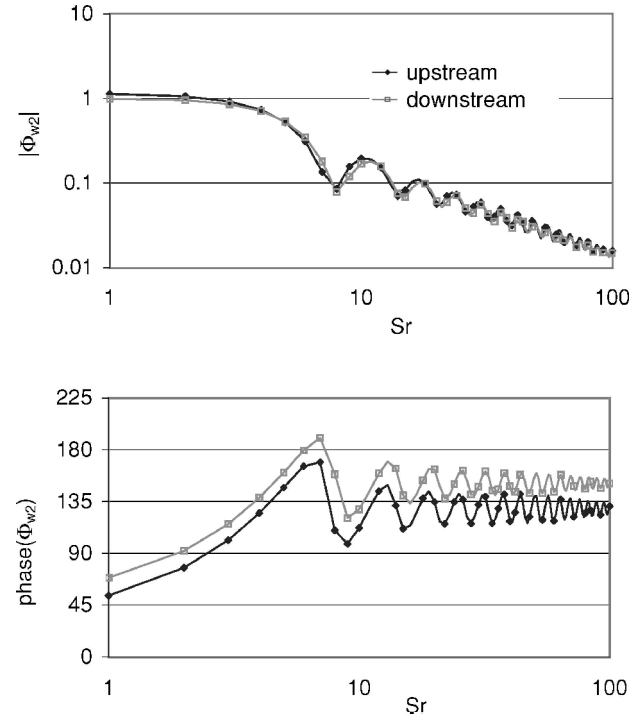


**Fig. 5 Comparison of Strouhal-number dependence of flame transfer function when flame is excited from upstream and downstream ($L/D_1$ = 1.59, $L/\lambda_1$ = 0.5, $D_2/D_1$ = 1, and $T_2/T_1$ = 6.67).**

of the two-dimensional results. These enhanced oscillations in the two-dimensional case are caused by less efficient cancellation in the

$$\int_0^1 \hat{u}_n'(\hat{r}) \exp(-i\,Sr\hat{r})\,\mathrm{d}\hat{r}$$

term because of nonuniformities in normal velocity along the flame.

The figure also shows that $\Phi_{w2}$ is nearly identical at the two different $L/\lambda_1$ and $L/D_1$ values. Thus, this result suggests that Strouhal number remains the dominant parameter controlling $\Phi_{w2}$, even in the two-dimensional case.

Figure 5 compares $\Phi_{w2}$ for the cases where the flame is excited from upstream and downstream. The graph shows that the results are nearly identical, that is, the transfer function exhibits a similar Strouhal-number dependence regardless of the direction of the incident wave. Figure 6 plots a similar result for the case where the diameter ratio of the expansion is two, $D_2/D_1 = 2$. As before, the results for up and downstream incidence are nearly identical, and the constant phase difference between the two results is caused by choice-of-reference velocity. Surprisingly, a comparison of this result with that in Fig. 5 shows that $\Phi_{w2}$ is nearly identical in this multidimensional geometry (an area change of four) to that calculated when there is no area expansion. This similarity is discussed further in the following.

The effects of varying the diameter ratio of the expansion at a fixed Strouhal number are illustrated in Fig. 7. The figure shows that the amplitude and phase of $\Phi_{w2}$ exhibit little dependence upon $D_2/D_1$. Because $\Phi_w$ and $\Phi_{w2}$ are related by the diameter ratio squared, the actual flame transfer function $\Phi_w$ does exhibit a strong dependence upon diameter ratio for downstream incidence.

Figure 8 plots the dependence of $\Phi_{w2}$ upon the dimensionless ratio of the flame length to acoustic wavelength $L/\lambda_1$ for a straight duct. The figure shows that the computed results for both up and downstream incidence are similar to the one-dimensional predictions for $L/\lambda_1 < 1$. As expected, the deviation between the one- and two-dimensional results increases with $L/\lambda_1$. Surprisingly, this agreement is still quite good for $L/\lambda_1$ values as high as 0.5. A similar comparison is plotted in Fig. 9, for a diameter ratio of $D_2/D_1 = 2$. As in the straight-duct case, the results for up and downstream incidence are qualitatively similar.

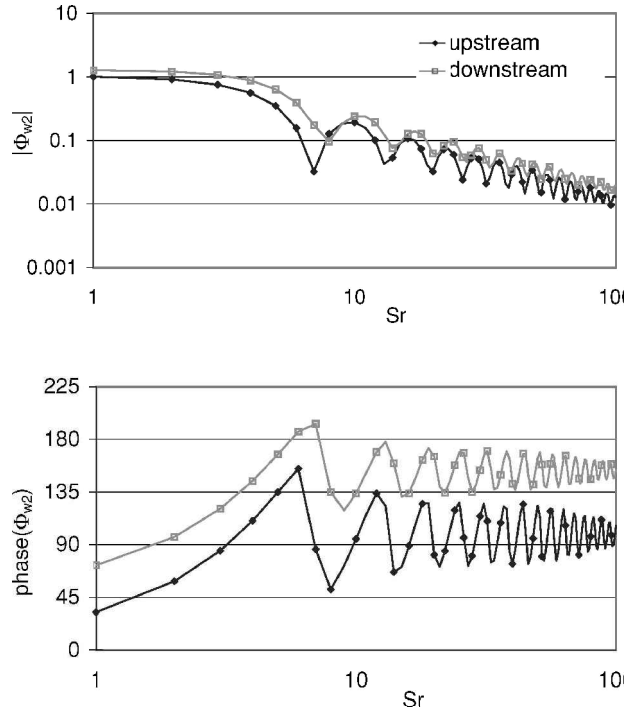


**Fig. 6 Comparison of Strouhal-number dependence of flame transfer function when flame is excited from upstream and downstream ($D_2/D_1$ = 2, $L/D_1$ = 1.59, $L/\lambda_1$ = 0.5, and $T_2/T_1$ = 6.67).**

Figure 10 plots the dependence of $\Phi_{w2}$ upon the dimensionless ratio of flame length to duct diameter $L/D_1$. As also noted earlier, the one-dimensional and computed results converge at the $L/D_1 = 0$ value because the geometry is one dimensional. These results appear to also approach a constant value for large $L/D_1$ values. In contrast to many of the prior results, the amplitude and phase of $\Phi_{w2}$ exhibit a strong dependence upon $L/D_1$, particularly when there is an area expansion (see Fig. 11). In addition, the characteristics of $\Phi_{w2}$

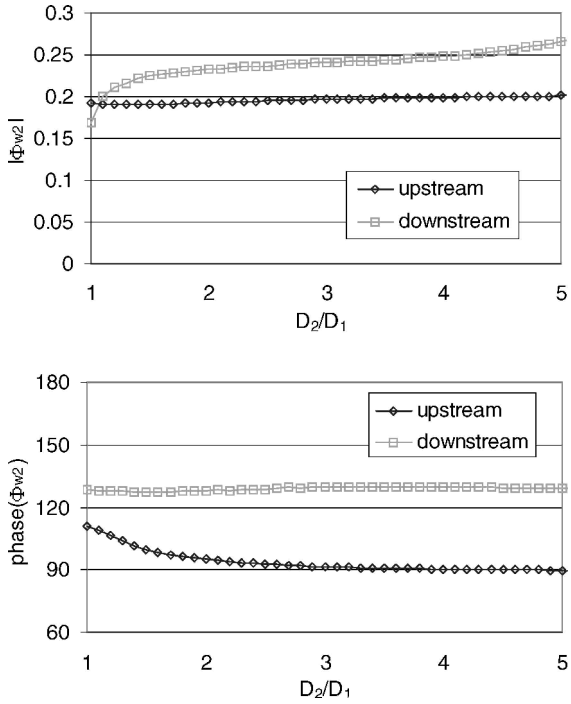


**Fig. 7 Dependence of flame transfer function on diameter ratio for cases where incident wave originates from upstream and downstream ($Sr = 10$, $L/D_1 = 1.59$, $L/\lambda_1 = 0.5$, and $T_2/T_1 = 6.67$).**

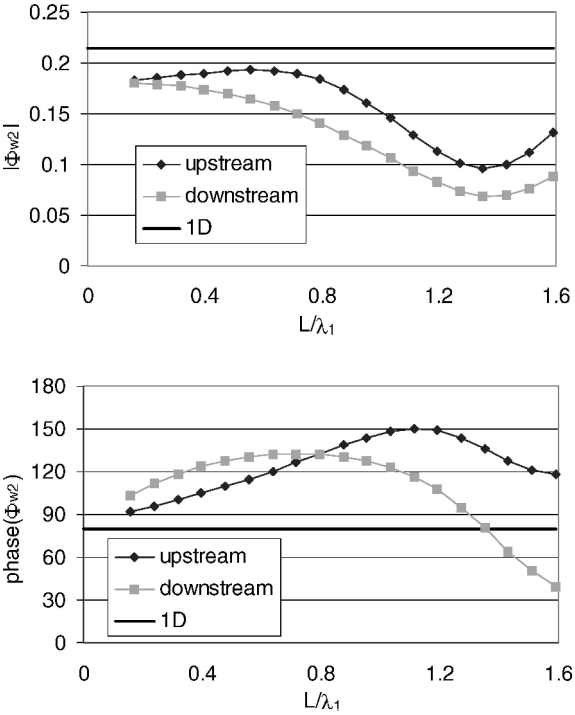


**Fig. 8 Dependence of magnitude and phase of flame transfer function upon $L/\lambda_1$ ($Sr = 10$, $L/D_1 = 1.59$, $T_2/T_1 = 6.67$, and $D_2/D_1 = 1$).**

strongly depend upon whether the incident wave originates from up or downstream.

Figure 12 plots the difference between $\Phi_{w2}$ and the one-dimensional transfer function $\Phi_{w,1-D}$ upon the temperature ratio across the flame $T_2/T_1$. It is reasonable to expect the temperature ratio to play an important role in these results because its departure from unity is ultimately what is responsible for creating deviations from one-dimensionality in the acoustic field in a straight duct. As expected, these two calculations converge in a straight duct at a

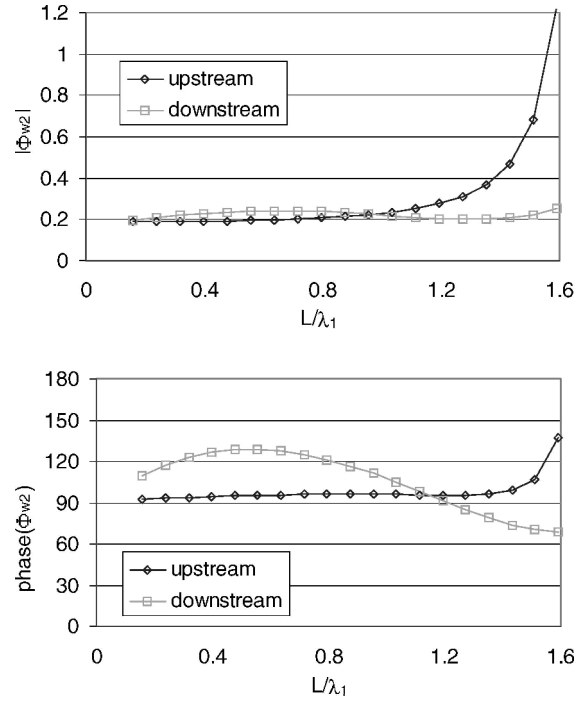


**Fig. 9 Dependence of magnitude and phase of flame transfer function upon $L/\lambda_1$ ($Sr = 10$, $L/D_1 = 1.59$, $T_2/T_1 = 6.67$, and $D_2/D_1 = 2$).**

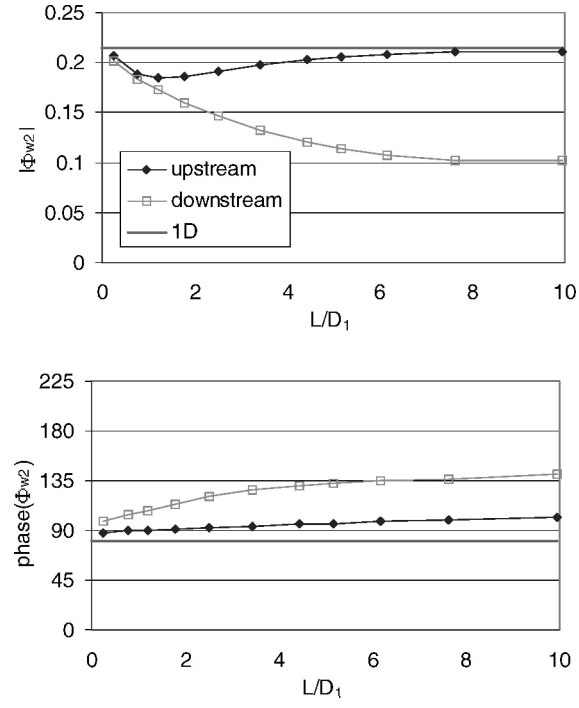


**Fig. 10 Dependence of magnitude and phase of flame transfer function upon $L/D_1$ ($Sr = 10$, $L/\lambda_1 = 0.1$, $T_2/T_1 = 6.67$, and $D_2/D_1 = 1$).**

unity temperature ratio. The deviations between the one- and two-dimensional transfer functions increasingly diverge with increased temperature ratio. For example, at a $T_2/T_1 = 6$ value they differ in amplitude by a factor of two and in phase by 10 deg. Figure 13 compares the computed $\Phi_{w2}$ in a nonstraight duct for up and downstream incident waves. As in many of the other results, the plots are quantitatively similar.

The preceding results show that the flame transfer function $\Phi_{w2}$ exhibits some dependence upon the parameters $L/\lambda_1$, $D_2/D_1$, $T_2/T_1$, and $L/D_1$. In most cases, however, the Strouhal-number dependence, which is captured by the one-dimensional model, appears

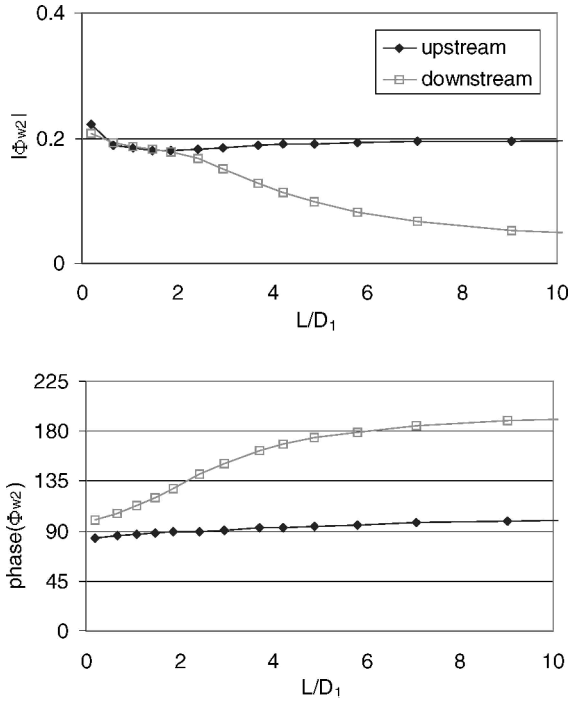


**Fig. 11 Dependence of magnitude and phase of flame transfer function upon $L/D_1$ ($Sr = 10$, $L/\lambda_1 = 0.1$, $T_2/T_1 = 6.67$, and $D_2/D_1 = 2$).**

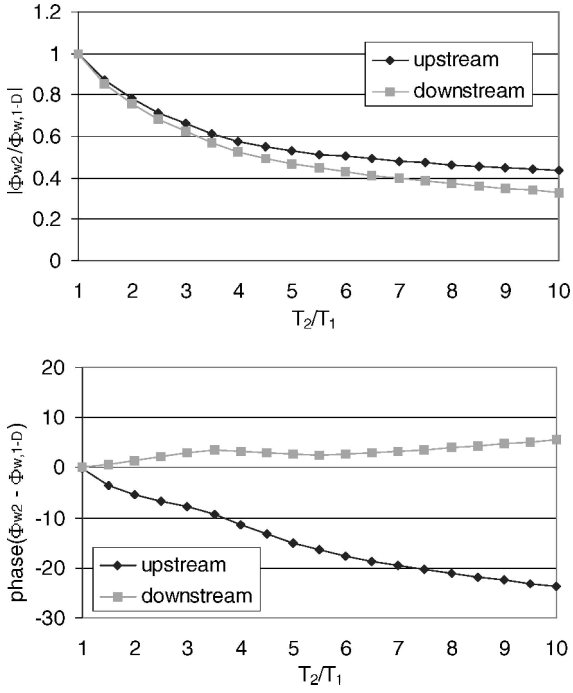


**Fig. 12 Difference between magnitude and phase of two- and one-dimensional flame transfer functions upon $T_2/T_1$ ($D_2/D_1 = 1$, $L/\lambda_1 = 0.1$, $L/D_1 = 1.59$, and $Sr = 20$).**

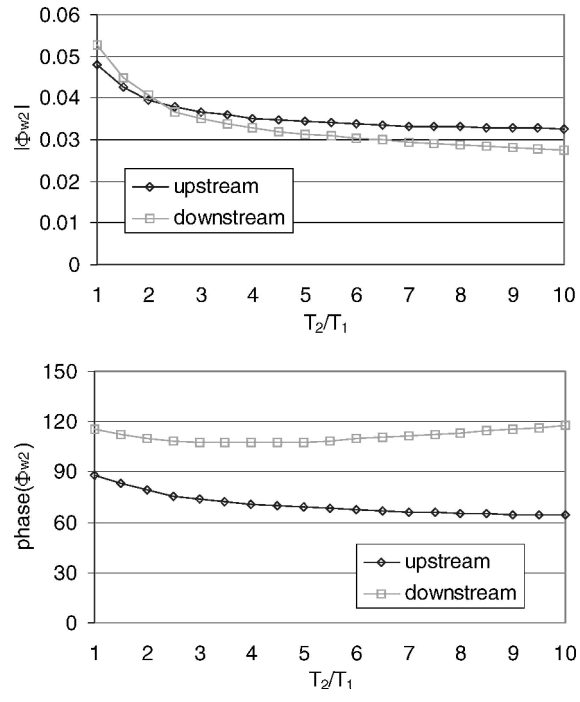


**Fig. 13 Dependence of flame transfer functions upon $T_2/T_1$ ($D_2/D_1 = 2$, $L/\lambda_1 = 0.1$, $L/D_1 = 1.59$, and $Sr = 20$).**

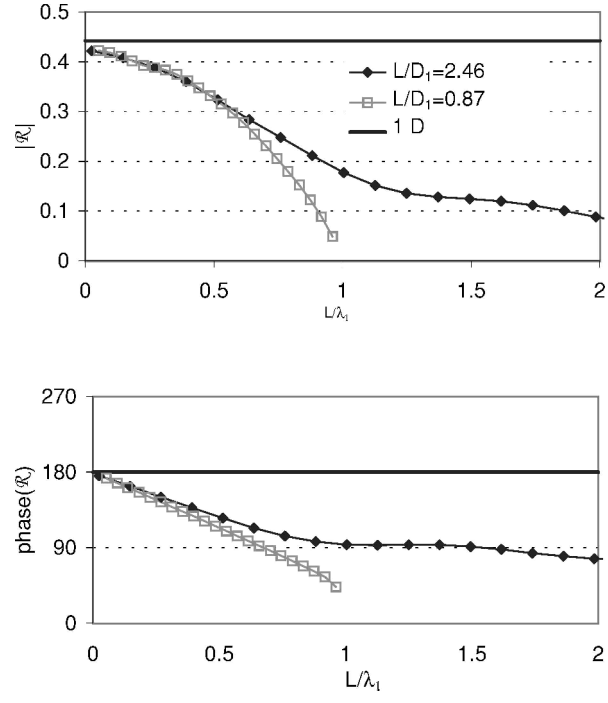


**Fig. 14 Dependence of magnitude and phase of the flame reflection coefficient upon $L/\lambda_1$. Phase was calculated by assuming the reflected wave originated axially at the flame base. Incident wave originates from upstream ($T_2/T_1 = 6.67$ and $D_2/D_1 = 1$).**

to have the largest qualitative influence upon $\Phi_{w2}$. It should be emphasized that these other parameters have an additional effect upon the transfer function, which is embedded in the reference velocity. Recall that the reference velocity was chosen as the plane-wave component of the acoustic wave on the incident side of the flame at the flame base. This reference velocity itself depends upon the plane-wave reflection coefficient [see Eq. (26)]. This reflection coefficient is affected by the two-dimensionality of the problem and depends upon the flame geometry (i.e., upon $D_2/D_1$ and $L/D_1$), temperature ratio, and $L/\lambda_1$. This dependence of $\Re$ upon $L/\lambda_1$ is shown in Fig. 14 for two different $L/D_1$ values. The one-dimensional reflection coefficient, obtained by continuity of pressure and volume flow considerations, is given by

$$\Re_{1-D} = \frac{1 - (D_2/D_1)^2\sqrt{T_2/T_1}}{1 + (D_2/D_1)^2\sqrt{T_2/T_1}} \tag{30}$$

Figure 14 shows that the magnitude and phase of the reflection coefficient are a function of the flame compactness ratio $L/\lambda_1$ and ratio of flame length to diameter $L/D_1$. The two-dimensional reflection coefficient deviates from the one-dimensional value with

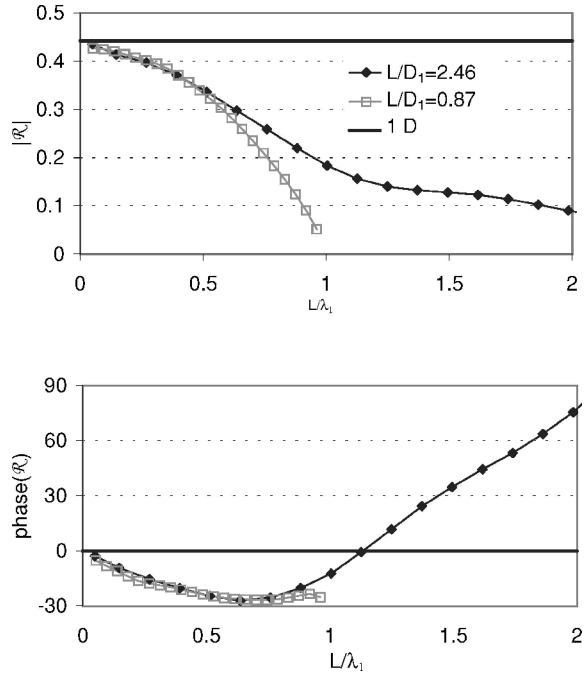


**Fig. 15 Dependence of the magnitude and phase of the flame reflection coefficient upon $L/\lambda_1$; incident waves originates from downstream ($T_2/T_1 = 6.67$ and $D_2/D_1 = 1$).**

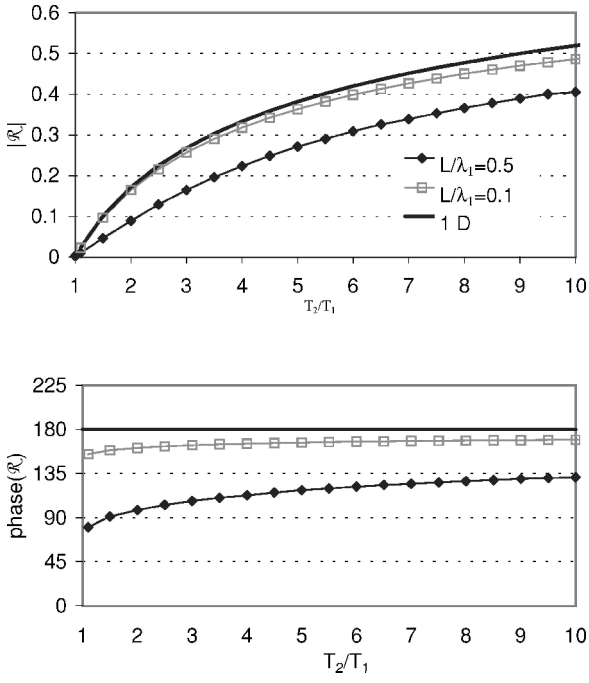


**Fig. 16 Dependence of the magnitude and phase of the flame reflection coefficient upon $T_2/T_1$. Incident wave originates from upstream ($D_2/D_1 = 1$ and $L/D_1 = 1.59$).**

increasing $L/\lambda_1$. The result also shows that the parameter $L/D_1$ does not affect the results for small $L/\lambda_1$ results, but becomes significant as the wavelength decreases. The results are similar for downstream incident waves (see Fig. 15). Figures 16 and 17 plot the dependence of the reflection coefficient upon the temperature ratio across the flame $T_2/T_1$ and diameter expansion ratio $D_2/D_1$. These figures show that the primary influence of these parameters is captured by the one-dimensional reflection coefficient. The one- and two-dimensional results exhibit similar dependencies upon these parameters, although, as expected, there is increasing deviation between them at larger $L/\lambda_1$ values.

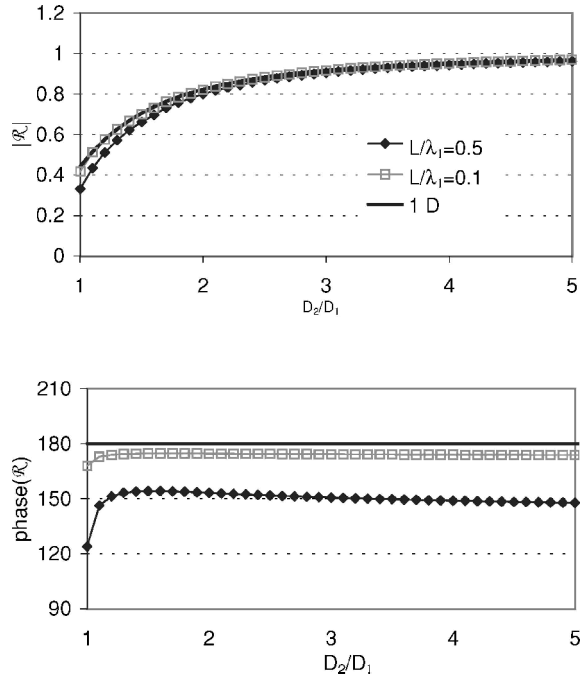


**Fig. 17 Dependence of the magnitude and phase of the flame reflection coefficient upon $D_2/D_1$. Incident wave originates from upstream ($T_2/T_1 = 6.67$ and $L/D_1 = 1.59$).**

## Discussion

Somewhat surprisingly, the preceding results show that incorporation of two-dimensional effects does not have substantial qualitative effects upon the transfer function calculations. This section considers the reasons for this agreement. In the subsequent discussion we consider the two limits where the flame is convectively compact, $Sr \ll 1$, and noncompact, $Sr \gg 1$, separately. Consider first the case where the flame is convectively compact. In this case expanding the exponential in Eq. (17) and retaining only the first-order term in the Strouhal number yields

$$\frac{A_f'}{\overline{A_f}} \approx 2\frac{\bar{U}}{S_u}\left[\int_0^1 \hat{u}_n'(\hat{r})\hat{r}\,\mathrm{d}\hat{r}\right] \propto \bar{Q}' \tag{31}$$

This equation shows that the normalized area fluctuations are directly related to the unsteady volume flow rate, $\hat{Q}'$ of gases through the flame. If the unsteady flowfield is incompressible, this volume flow rate is invariant, whether it is calculated directly at the flame surface or at positions sufficiently in front or behind it, where the acoustic field is one dimensional (see Fig. 3). Because one-dimensional calculations can be used to determine this volume flow rate sufficiently up or downstream of the flame, two-dimensional effects will not alter approximate one-dimensional results if the flowfield is incompressible. Such an incompressible limit is most appropriate if the flame is acoustically compact because the perturbation properties do not change significantly over length scales on the order of the flame length. Thus, this discussion shows that deviations between one- and two-dimensional results for small Strouhal numbers are caused by gas compression in the flame region. It is expected that the amount of compression is directly related to the parameter $L/\lambda_1$. This is likely responsible for the $L/\lambda_1$ effects upon the flame transfer function shown in Figs. 8 and 9.

Consider next the $Sr \gg 1$ case. In this case the first term in Eq. (17) is much smaller than the second because acoustic disturbances vary over length scales much longer than the convective wavelength. Thus, the rapid oscillations in the $\exp(-iSr\hat{r})$ term relative to the $u_n'$ term cause this first term to integrate to nearly zero. The decreasing effect of this oscillatory term can be seen in Figs. 4–6. It can be seen that the remaining term

$$\int_0^1 \hat{u}_n'(\hat{r})\,\mathrm{d}\hat{r}$$

is not directly related to the volume flow rate through the flame, as it was before. However, if the acoustic field is incompressible and spatially uniform along the flame surface (but not necessarily one dimensional), then evaluation of the resulting term yields the same result as a one-dimensional calculation. Thus, deviation between the one- and two-dimensional results in the $Sr \gg 1$ case are caused by flow compressibility and spatial nonuniformity. It is anticipated that the parameters $L/\lambda_1$ and $L/D_1$ dominate the former and latter effects, that is, the flowfield is more incompressible at low $L/\lambda_1$ and more uniform at low $L/\lambda_1$ and $L/D_1$, and, hence, approximate one-dimensional calculations will be more accurate.

## Conclusions

The preceding results show that the acoustic field near the flame is two dimensional, even for straight-duct geometries. However, in most cases this two-dimensionality does not exert substantial qualitative differences between one- and two-dimensional calculations. Thus, these results clarify the reasons behind the rather unexpected agreement between a simplified one-dimensional theory and measurements.

## References

[1]Shih, W. P., Lee, J., and Santavicca, D., "Stability and Emissions Characteristics of a Lean Premixed Gas Turbine Combustor," *Proceedings of the Combustion Institute*, Vol. 26, 1996, pp. 2771–2778.

[2]Markstein, G. H. (ed.), *Nonsteady Flame Propagation*, Pergamon Press, New York, 1964, Chap. 8.

[3]Marble, F. E., and Candel, S. M., "An Analytical Study of the Non-Steady Behavior of Large Combustors," *Proceedings of the Combustion Institute*, Vol. 17, 1978, pp. 761–769.

[4]Yang, V., and Culick, F. E. C., "Analysis of Low Frequency Combustion Instabilities in a Laboratory Ramjet Combustor," *Combustion Science and Technology*, Vol. 45, 1985, pp. 1–25.

[5]Dowling, A., "Nonlinear Self Excited Oscillations of a Ducted Flame," *Journal of Fluid Mechanics*, Vol. 346, 1997, pp. 271–290.

[6]Fleifil, M., Annaswamy, A. M., Ghoniem, Z. A., and Ghoniem, A. F., "Response of a Laminar Premixed Flame to Flow Oscillations: A Kinematic Model and Thermoacoustic Instability Results," *Combustion and Flame*, Vol. 106, No. 4, 1996, pp. 487–510.

[7]Pierce, A. D., *Acoustics: An Introduction to Its Physical Principles and Applications*, Acoustical Society of America, New York, 1994.

[8]Lee, D. H., and Lieuwen, T., "Acoustic Nearfield Characteristics of a Conical, Premixed Flame," *Journal of the Acoustical Society of America*, Vol. 113, No. 1, 2003, pp. 167–177.

[9]Ducruix, S., Durox, D., and Candel, S., "Theoretical and Experimental Determinations of the Transfer Function of a Laminar Premixed Flame," *Proceedings of the Combustion Institute*, Vol. 28, 2000, pp. 765–772.

[10]Correa, S. M., "A Review of NOx Formation Under Gas-Turbine Combustion Conditions," *Combustion Science and Technology*, Vol. 87, No. 1–6, 1992, pp. 329–362.

[11]Turns, S., *An Introduction to Combustion*, McGraw–Hill, New York, 2000.

[12]Matalon, M., and Matkowsky, B. J., "Flames as Gas Dynamics Discontinuities," *Journal of Fluid Mechanics*, Vol. 124, 1982, pp. 239–259.

[13]Lieuwen, T., "Theoretical Investigation of Unsteady Flow Interactions with a Premixed Planar Flame," *Journal of Fluid Mechanics*, Vol. 435, 2001, pp. 289–303.

[14]McIntosh, A. C., "Pressure Disturbances of Different Length Scales Interacting with Conventional Flames," *Combustion Science and Technology*, Vol. 75, No. 1, 1991, pp. 287–309.

[15]Lieuwen, T., "Experimental Investigation of Limit Cycle Oscillations in an Unstable Gas Turbine Combustor," *Journal of Propulsion and Power*, Vol. 18, No. 1, 2002, pp. 61–67.

[16]Poinsot, T., Veynante, D., Bourienne, F., Candel, S., Esposito, E., and Surget, J., "Initiation and Suppression of Combustion Instabilities by Active Control," *Proceedings of the Combustion Institute*, Vol. 22, 1988, pp. 1363–1370.

[17]Lovett, J., and Uznanski, K., "Prediction of Combustion Dynamics in a Staged Premixed Combustor," American Society of Mechanical Engineers, Paper GT-2002-30646, June 2000.

[18]Baillot, F., Durox, D., and Prud'homme, R., "Experimental and Theoretical Study of a Premixed Vibrating Flame," *Combustion and Flame*, Vol. 88, No. 2, 1992, pp. 149–168.

[19]Crighton, D. G., "The Kutta Condition in Unsteady Flow," *Annual Review of Fluid Mechanics*, Vol. 17, 1985, pp. 411–445.

[20]Howe, M. S., *Acoustics of Fluid-Structure Interactions*, Cambridge Univ. Press, Cambridge, England, U.K., 1998.

[21]Bechert, D. W., "Sound Absorption Caused by Vorticity Shedding, Demonstrated with a Jet Flow," *Journal of Sound and Vibration*, Vol. 70, No. 3, 1980, pp. 389–405.

[22]Wu, T. W., *Boundary Element Acoustics: Fundamentals and Computer Codes*, WIT, Boston, MA, 2000.

[23]Brebbia, C. A., Silva, J. J., and Partridge, P. W., "Computational Formulation," *Boundary Element Methods in Acoustics*, edited by R. D. Ciskowski, and C. A. Brebbia, Computational Mechanics Publications, Boston, 1991, pp. 13–60.